Interfacial Microstructures in Martensitic Transitions: From Optical Observations to Mathematical Modeling

Hanuš Seiner,[1,2]* **Ondřej Glatz,**[1,2] **& Michal Landa**[1]

[1]*Institute of Thermomechanics, Academy of Sciences of the Czech Republic, 18 200 Prague 8, Czech Republic*

[2]*Faculty of Nuclear Sciences and Physical Engineering, Czech Technical University in Prague, 120 00 Prague 2, Czech Republic*

ABSTRACT

We present a construction of a mathematical model of an interfacial microstructure (i.e., microstructure forming at the phase interface between austenite and martensite) in a single crystal of Cu-Al-Ni shape memory alloy. In the first part of the article, the experiment is briefly outlined and the compatibility of the experimentally observed microstructures is analyzed, showing that the observed X-interfaces cannot be compatible without the presence of elastic strains. Then, the elastic strains in the microstructure are evaluated by finite element method, whereby the elastic coefficients of finely microstructured regions are obtained by homogenization. The significant influence of the choice of the geometry on the numerical results is shown and discussed.

KEYWORDS

martensitic transition, shape memory alloys, X-interface, Cu-Al-Ni

*Address all correspondence to hseiner@it.cas.cz.

1. INTRODUCTION

All the unique thermomechanical properties of shape memory alloys (SMAs), such as the shape memory effect, superelasticity, or pseudoplasticity, are commonly known to result from reversible martensitic transitions taking place in these materials under proper mechanical and/or thermal loading [1]. Similarly, most of these effects would be impossible without the ability of the low-temperature (martensitic) phases of SMAs to form geometrically ordered mixtures of different variants, i.e., of martensites rotated variously with respect to the parent (high-temperature, austenitic) crystal lattice. These mixtures are usually called *martensitic microstructures* [2], and their existence is enabled by reversible twinning of martensite (we will refer to them further in text as *twinned structures* or simply *twins*). According to the theory developed by Ball and James (see [3, 4]), the observed domain Ω of an SMA single crystal always forms such microstructure that the entire free energy

$$\Phi = \int_\Omega \varphi(\nabla \mathbf{y}(\mathbf{x}), T) \mathrm{d}V \qquad (1)$$

is minimal for given boundary conditions at $\partial\Omega$. Here, $\mathbf{x}$ denotes the reference configuration (which is usually chosen identically with the unrotated austenite phase), $\mathbf{y}$ is the deformed configuration, T is temperature, and φ is the multiwell free-energy density. In a stress-free state, this energy density has equivalently deep minima in the deformation gradients $\nabla \mathbf{y}(\mathbf{x})$, corresponding to all particular variants of martensite, and one minimum in $\nabla \mathbf{y}(\mathbf{x}) \in \mathrm{SO}(3)$ (i.e., for austenite), which can be either deeper (at T higher than some critical temperature) or have the same or lower depth than the martensitic wells (at the critical temperature and below it). For most of the boundary conditions, the minimizer of (1) cannot be directly obtained, but the minimum (or infimum) can be approached by construction of minimizing sequences, which is an equivalent of fine microstructuring in the real material (for more details, see, e.g., [5]). The most usually observed homogeneous microstructure (the first-order laminate consisting of two variants of martensite forming parallel lamina of alternate thicknesses) corresponds to the simplest possible minimizing sequence for a wide range of boundary conditions [6].

The concept of microstructures as minimizing sequences of (1) has successfully explained many features observed in real single crystals of SMAs–above all, the formation of fine laminates at planar austenite-to-martensite interfaces, called *habit planes*. There are, however, few cases where this theory is not able to predict exactly what microstructure will form and how it will develop in time under given external mechanic and thermal loadings. Or, in other words, under some special mechanic and thermal loadings, microstructures can develop that do not minimize (1) for prescribed boundary conditions. An apparent example of such a case is the shape recovery process (i.e., the thermally induced transition from a mechanically stabilized martensite [7] to austenite) of Cu-Al-Ni single crystals, recently reported in [8]. In this case, the transition front has a form of the so-called X-interface (microstructure first documented in the In-Th alloy by Basinski and Christian [9]). As shown by Ruddock [10] for the In-Th system (and as it will be shown for Cu-Al-Ni in this article), this microstructure cannot achieve compatibility without elastic strains and thus cannot be an energy minimizer of (1) at the transition temperature for the free boundary conditions. However, the X-interfaces observed by the authors of [8] in Cu-Al-Ni were pretty stable in a whole range of temperatures and did not exhibit any tendency to get rebuilt into true energy minimizers. A similar situation appears for so-called wedge microstructures often observed during thermally induced transitions from austenite to self-accommodated martensite. In [11], the authors have given a detailed analysis of this microstructure, showing again that the compatibility can be attained only by the presence of elastic strains.

This article aims to discuss the X-interfaces in Cu-Al-Ni single crystals reported in [8], with a focus on determination of the elastic strain fields enabling such microstructure to achieve compatibility. This includes a detailed analysis of the experimentally observed microstructures, construction of a numerical model such that it copies the real geometry in an optimal way (although some simplifications are necessary), and solution of the resulting elasticity problem. In general, the mathematical modeling of martensitic microstructure is always a strongly multiscale problem [12], as the deformed configuration $\mathbf{y}$ can be always decomposed as follows:

$$\mathbf{y}(\mathbf{x}) = (\mathbf{y}_{\mathrm{elast}} \circ \mathbf{y}_{\mathrm{trans}})(\mathbf{x}) \qquad (2)$$

where the elastic strains (given by mapping $\mathbf{y}_{\mathrm{elast}}$) are incomparably smaller than the transformation strains (mapping $\mathbf{y}_{\mathrm{trans}}$), i.e., strains given by the martensitic transition itself. In this article (analogously to [11]), we suppress the multiscale character of this problem by taking the mapping $\mathbf{y}_{\mathrm{trans}}$ directly from the experimental observations, instead of from the condition of minimality of (1). Then, the strain fields are determined as minimizers of (1) for given $\mathbf{y}_{\mathrm{trans}}$. Such an optimization problem is incomparably simpler than the solution of models capturing fully the constitutive behavior of the material [13–16]. On the other hand, the multiscale character cannot be fully avoided, as the analyzed microstructures include different length scales: They consist of finely twinned regions, which must be homogenized (both in their deformation gradients $\nabla \mathbf{y}_{\mathrm{trans}}$ and in their elastic properties) prior to their own numerical treatments.

2. EXPERIMENT

2.1 Examined Material

The Cu-Al-Ni alloy used in the experiments reported in [8] and in this article is a shape memory alloy undergoing a cubic-to-orthorhombic transition (for more details, see, e.g., [17], and the extensive list of references therein; for a comprehensice summary of microstructures forming in single crystals of this alloy, see [18]). For this kind of transition, the austenite phase can transform into six different variants of martensite. We will denote these variants in this article by arabic numbers 1 to 6, and use the same numbering as in [19], where, also, the Bain matrices $\mathbf{U}_{1,\ldots,6}$ for these variants can be found. As none of these variants can form a compatible interface with austenite (i.e., the compatibility equation [3, 4]

$$\mathrm{rank}\,(\mathbf{Q}\mathbf{U}_i - \mathbf{I}) = 1 \qquad (3)$$

cannot be fulfilled for any i and any $\mathbf{Q} \in \mathrm{SO}(3)$), all the phase interfaces in this alloy can exist only between austenite and a twinned structure of martensite. According to [2], the martensitic phase of this alloy can form twins in three different twinning systems. These are the *compound twins*, where the twinning plane is a plane of mirror symmetry between the two involved variants, and *type I* and *type II twins*, where it is not. Another difference between

these twinning systems is that whereas the fine laminates of type I and type II twins can form compatible interfaces with austenite (i.e., there exist matrices $\mathbf{Q}_A \in \mathrm{SO}(3)$ and $\mathbf{Q}_B \in \mathrm{SO}(3)$ and a scalar parameter λ such that

$$\mathrm{rank}\,(\lambda\mathbf{Q}_A\mathbf{U}_A + (1-\lambda)\mathbf{Q}_B\mathbf{U}_B - \mathbf{I}) = 1 \qquad (4)$$

where A and B is a pair of variants able to form type I or type II twins), the laminates of compound twins cannot. For this reason, any transition from a single variant of martensite into austenite cannot proceed without formation of laminates of type I or type II twins at the transition front, i.e., without formation of the so-called *interfacial microstructures* (see [8] for a more exact definition).

For completeness, we will list here also the transition temperatures as determined for the examined material by DSC measurements: The martensite start temperature was $M_S = -5°C$, the martensite finish temperature was $M_F = -22°C$, the austenite start temperature was $A_S = 26°C$, and the austenite finish temperature was $A_F = 52°C$.

2.2 Experimental Procedure

The X-interfaces in Cu-Al-Ni single crystals were prepared by the following experimental procedure (for more details, see [8]). A specimen (15 mm long and 5×5 mm thick prismatic bar of single crystal of austenite oriented along the [001] direction) was uniaxially compressed until it transformed into mechanically stabilized 2H martensite. Due to the mechanical stabilization (i.e., the inability of the obtained martensite to form directly compatible interfaces with austenite), the specimen did not return to austenite after the loading was removed, but remained in martensite even when it was heated over the A_S temperature. The obtained martensitic bar was a single variant of martensite including a negligible (less than 5%) volume fraction of another variant in the form of thin plates running through the specimen and forming compound twins with the major variant. In one corner of the specimen, a small nucleus of the austenite phase was induced by strong localized heating (using a gas lighter). Then, the whole specimen was heated by being immersed into a warm (60°C) water bath, which induced a growth of austenite from the nucleus. As soon as the transition front reached approximately the middle of the specimen, the specimen was removed from

the bath and cleaned and was cooled down by ethyl alcohol. The formed microstructure (stable at room temperature) was observed by optical microscopy.

Repeatedly, the transition front was arranged as shown in Fig. 1, forming the so-called X-interface, consisting of two mutually intersecting habit planes separating austenite from twinned regions of martensite and another pair of mutually intersecting interfaces separating these twinned regions from the original stabilized martensite. The interfaces between the twinned regions and the original stabilized martensite were parallel (or very close to parallel) to the twinning planes seen inside the twinned regions. The whole X-interface was mirror symmetric about the $(1\bar{1}0)$ plane in austenite.

2.3 Compatibility Analysis

Schematically, the geometry of the X-interface is sketched in Fig. 2. For simplicity, we will assume the stabilized martensite to be a single variant.[1] Under such an assumption, the microstructure consists of austenite and three variants of martensite only (denoted A, B, and C in Fig. 2). To analyze the compatibility, the particular variants of martensite and twinning systems appearing in the microstructure were identified. Optical micrographs of all faces of the specimen were taken, and the angles between the habit planes, twinning planes, and the edges of the specimen were measured. A script written in MATLAB was used to compute orientations of habit planes and twinning planes of all possible combinations of variants able to form X-interfaces, and to find which of these combinations fits the optical micrographs optimally. By this script, the twinning systems observed in the microstructure were identified as type II twinning planes of 2H martensite. The involved variants identified by this script were no. 4 and no. 6, forming one type II laminate, and no. 2 and no. 6, forming the second one. This induced that the stabilized martensite (i.e., the variant involved in both laminates) must be no. 6, which was verified by X-ray measurements (Laue method).

---

[1] As shown in [8] by a numerical example, the negligible amount of compound twins in the real specimen does not have any measurable effect on the orientation of the habit planes, etc.
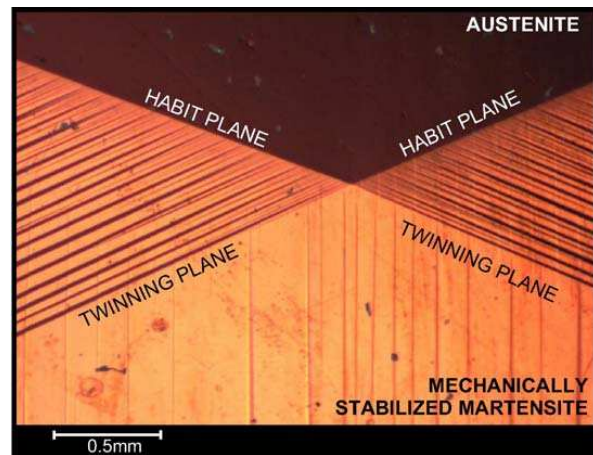

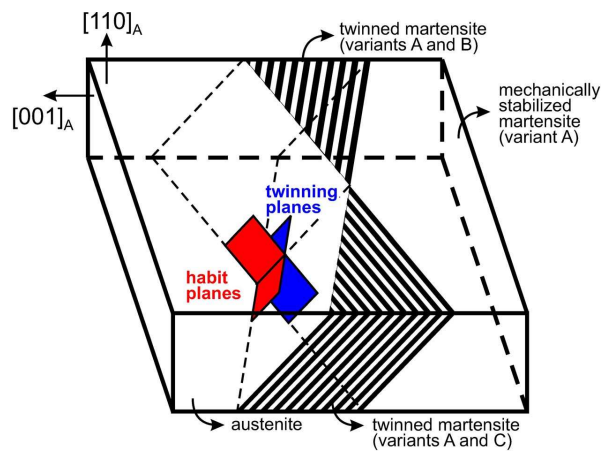**FIGURE 1.** Optical micrograph of the X-interface in Cu-Al-Ni

FIGURE 2. Geometry of the X-interfaces observed in Cu-Al-Ni single crystals

For general analysis of the compatibility of the microstructure, we will return to the notation introduced in Fig. 2 (now $A \sim$ no. 6, $B \sim$ no. 4, and $C \sim$ no. 2). The variants A and B form a laminate of type II twins, which borders on the austenite over a habit plane (let us denote a normal vector to this plane by $\mathbf{n}$) and pure variant A over the A-B type II twinning plane. Similarly, variant A forms a type II laminate with variant C, and this laminate borders over another habit plane (normal vector orientation $\hat{\mathbf{n}}$) on the austenite, and over the A-C type II twin-

ning plane on pure variant A. For $\mathbf{U}_A$, $\mathbf{U}_B$, and $\mathbf{U}_C$ being the Bain tensors of particular variants $\mathbf{b}$ and $\hat{\mathbf{b}}$ being the shearing vectors corresponding to transitions at habit planes with normals $\mathbf{n}$ and $\hat{\mathbf{n}}$, and λ and $\hat{\lambda}$ being the volume fractions of variant A in the two considered laminates, we can write the compatibility equations at both habit planes as

$$\mathbf{I} - (\lambda \mathbf{Q}_A \mathbf{U}_A + (1 - \lambda) \mathbf{Q}_B \mathbf{U}_B) = \mathbf{b} \otimes \mathbf{n} \quad (5)$$

$$\mathbf{I} - \left(\hat{\lambda} \hat{\mathbf{Q}}_A \mathbf{U}_A + (1 - \hat{\lambda}) \mathbf{Q}_C \mathbf{U}_C \right) = \hat{\mathbf{b}} \otimes \hat{\mathbf{n}} \quad (6)$$

where $\mathbf{Q}_A$, $\mathbf{Q}_B$, $\hat{\mathbf{Q}}_A$, and $\mathbf{Q}_C$ are rotations between austenite and particular variants of martensite involved in the microstructure. Simultaneously, the compatibility conditions must be fulfilled at the type II twinning planes, i.e., there must exist such shearing vectors $\mathbf{a}$ and $\hat{\mathbf{a}}$ such that

$$\mathbf{Q}_A \mathbf{U}_A - \mathbf{Q}_B \mathbf{U}_B = \mathbf{a} \otimes \mathbf{m} \quad (7)$$

$$\hat{\mathbf{Q}}_A \mathbf{U}_A - \mathbf{Q}_C \mathbf{U}_C = \hat{\mathbf{a}} \otimes \hat{\mathbf{m}} \quad (8)$$

where $\mathbf{m}$ and $\hat{\mathbf{m}}$ are unit normals to the A–B and A–C twinning planes.

Two general conditions can be formulated, under which the whole microstructure is compatible without elastic strains. The first condition is that the pure variant A in the stabilized region must be rotated with respect to austenite equivalently as in the laminates since it borders an the variants B and C over the A–B and B–C twinning planes. This directly induces that $\hat{\mathbf{Q}}_A = \mathbf{Q}_A$. However, as it can be easily checked numerically, this condition is not satisfied for our material. For the lattice parameters taken from [18], we can calculate the difference between these two rotations $\hat{\mathbf{Q}}_A^{-1} \mathbf{Q}_A = \hat{\mathbf{Q}}_A^{\mathrm{T}} \mathbf{Q}_A$ (the all rotation matrices in (5) and (6) as well as the volume fractions can be obtained by algorithms described in [3, 4]). In a quaternion representation, the difference $\hat{\mathbf{Q}}_A^{\mathrm{T}} \mathbf{Q}_A$ equals a rotation by $6.6°$ around a direction close to $[77\bar{3}]$ in austenite.

The second condition is that the habit planes and the twinned-to-detwinned interfaces must intersect in the same line, i.e.,

$$(\mathbf{n} \times \hat{\mathbf{n}}) \| (\mathbf{m} \times \hat{\mathbf{m}}) \quad (9)$$

(providing that the twinned-to-detwinned interfaces are exactly equal to the twinning planes). Again, this condition cannot be fulfilled for the examined Cu-Al-Ni alloy. The difference between

$\mathbf{n} \times \hat{\mathbf{n}}$ and $\mathbf{m} \times \hat{\mathbf{m}}$ determined numerically for the lattice parameters taken from [18] is $2.2°$. The incompatibility of the X-interface can be also illustrated by the difference between vectors $\mathbf{m} \times \mathbf{n}$ and $\hat{\mathbf{m}} \times \hat{\mathbf{n}}$, which is, for the same lattice parameters, equal to $7.2°$.

If the twinned-to-detwinned interfaces are declined from the orientation of the corresponding type II twinning planes, condition (9) can be fulfilled, but in such case, the presence of elastic strains is necessary to ensure compatibility along the twinned-to-detwinned interfaces.

3. MATHEMATICAL MODELING

The revealed difference from compatibility must be compensated by the presence of elastic strains. In this section, we will try to determine these strain fields by the finite element method (FEM). Unlike in most FEM models of SMAs [20, 21], the elements used in this case do not have to incorporate the constitutive behavior of the material, and thus common FEM solvers can be used.

3.1 Simplified Geometry Used in the Model

As mentioned in the introduction, the FEM model of the interfacial microstructure cannot be constructed for exactly the geometry obtained from the experiments, and some simplifications are necessary. The reason is that the difference between $\mathbf{n} \times \hat{\mathbf{n}}$ and $\mathbf{m} \times \hat{\mathbf{m}}$ (i.e., between the intersection of the habit planes and the type II twinning planes) is comparable to the accuracy with which the real angles from the optical micrographs are determined, so the exact orientation of the crossing line is unknown. Moreover, there is no physical justification for the assumption that the twinned-to-detwinned interfaces are exactly planar.

One possible way to solve this problem is to parametrize the orientations (and possibly also the shapes [22]) of all interfaces to find which geometry results in minimal energy (1). However, as the X-interface analyzed in this article is *a priori* not an energy minimizer of (1), such an approach would be completely unjustified. Instead, we decided to evaluate the elastic strain fields for four different simplified geometries (SG). These are ($\mathbf{c}$ is always a unit vector determining the direction of the crossing line) as follows:

- **SG 1:** where the crossing line lies in the intersection of the habit planes (i.e., $\mathbf{c} = \mathbf{n} \times \hat{\mathbf{n}}$), and the planar twinned-to-detwinned interfaces are chosen as such planes containing $\mathbf{c}$ that the declinations of the normal vectors to these planes from $\mathbf{m}$ and $\hat{\mathbf{m}}$ are minimal. In this case, the compatibility conditions at the habit planes (5) and (6) are fulfilled, but not at the twinned-to-detwinned interfaces, where the elastic strains must ensure the compatibility.

- **SG 2:** where the crossing line lies in the intersection of the type II twinning planes (i.e., $\mathbf{c} = \mathbf{m} \times \hat{\mathbf{m}}$), and the planar twinned-to-austenite interfaces are chosen as such planes containing $\mathbf{c}$ that the declinations of the normal vectors to these planes from $\mathbf{n}$ and $\hat{\mathbf{n}}$ are minimal. Here the compatibility conditions at the twinned-to-detwinned interfaces are identical to (7) and (8) and are fulfilled, whereas the compatibility at the twinned-to-austenite interfaces (which are slightly declined from the habit planes determined by conditions (5) and (6)) must be enabled by the presence of elastic strains.

- **SG 3:** where the crossing line lies in the intersection of one habit plane and one type II twinning plane (i.e., $\mathbf{c} = \mathbf{n} \times \mathbf{m}$), and the remaining twinned-to-austenite and twinned-to-detwinned interfaces are chosen as such planes containing $\mathbf{c}$ that the declinations of the normal vectors to these planes from $\hat{\mathbf{n}}$ and $\hat{\mathbf{m}}$ are minimal. In this case, only conditions (5) and (7) are fulfilled, so the region with the A–B laminate is compatibly connected to both austenite and the stabilized martensite.

- **SG 4:** is mirror symmetric to SG 3 (i.e., $\mathbf{c} = \hat{\mathbf{n}} \times \hat{\mathbf{m}}$) with the region with the A–C laminate compatibly connected to both austenite and the stabilized martensite.

The real geometry of the microstructure can be expected to be somewhere between the simplified geometries SG 1÷4.

The simplified geometries are shown in Fig. 3. For parametrization of the location of the crossing line in each geometry, the distance of the intersection of the crossing line with the chosen face from a
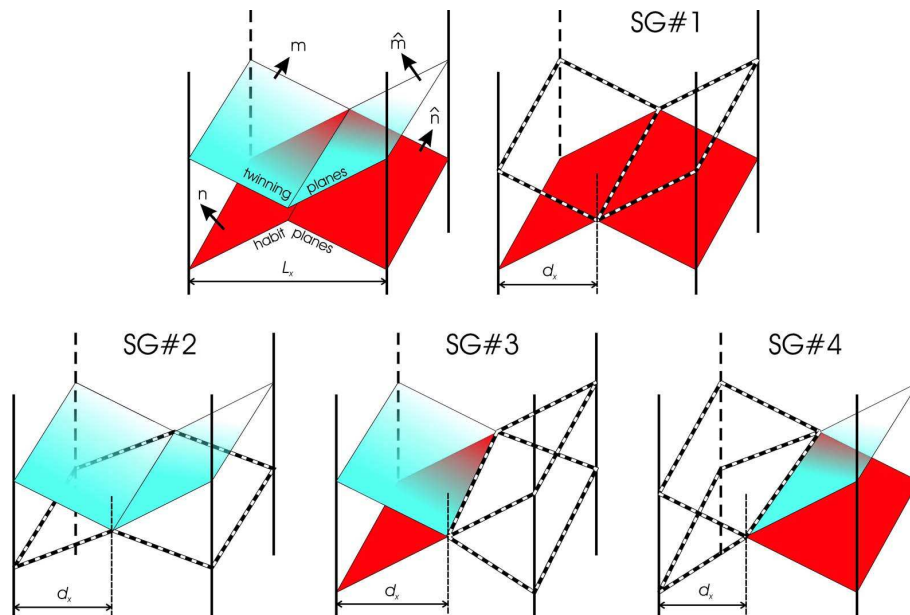

FIGURE 3. Simplified geometries SG 1 to SG 4. Filled (shaded) planes are always those compatible without elastic strains, planes outlined by the dashed lines are compatible only due to elastic strains. The first scheme shows the orientation of unit vectors $\mathbf{m}$, $\mathbf{n}$, $\hat{\mathbf{m}}$ and $\hat{\mathbf{n}}$, and the choice of L_x. Parametrization by d_x is shown for each geometry

chosen edge of the specimen was used. For this distance, denoted by d_x, the dimensionless ratio d_x/L_x (where L_x is the width of the chosen face in austenite; see Fig. 3) has the following sense: The geometries SG 1 and SG 2 are symmetric for $d_x/L_x = 1/2$, the geometry SG 3 is fully compatible for $d_x/L_x = 1$, and SG 4 is fully compatible for $d_x/L_x = 0$.

3.2 Elasticity of Pure and Twinned Regions

To evaluate the elastic stress and strain fields in the X-interface of known geometry, the elastic coefficients of all materials contained in the microstructure must be known. For austenite and stabilized martensite (single variant), the elastic coefficients can be found in [19], where the methodology of how these coefficients were determined from ultrasonic measurements is also described in details. Austenite exhibits cubic elastic anisotropy, which means that it can be fully described by three independent elastic coefficients. A single variant of martensite is orthorhombic; for this class of symmetry, the number of independent elastic coefficients is nine (e.g., [23]).

Theoretically, the coefficients for austenite and a single variant of martensite would be sufficient for evaluation of the stresses and strains in any microstructure. However, in our case of the X-interface, such an approach would require us to treat all the lamina within the twinned regions as individual components with prescribed geometries and elastic properties. This would turn the evaluation of the stress and strain fields into a strongly multiscale problem, as the thicknesses of individual layers are incomparably smaller than other dimensions of the microstructure. At the length scales comparable to the dimensions of the specimen, the twinned regions can be treated as homogeneous, with elastic properties obtained by some homogenization procedure.

The homogenization procedure used here for evaluation of all elastic coefficients (21 independent coefficients, as the resulting material is triclinic) of the type II twinned structures of CuAlNi was very similar to those used for evaluation of elastic coefficients of layered macroscopic composites (e.g., [24]). The details on the procedure can be found in [25] and in [26]. Here, thus, we restrict ourselves to a short outline of the algorithm and the obtained results only.

The procedure homogenizes a first-order laminate of two variants (denoted, again, A and B), which are connected by relation (7). In the natural coordinate system of variant A (i.e., the system aligned with the orthorhombic axes of this variant), the elastic coefficients of variant B can be obtained by rotating the tensor of elastic coefficients of variant A by two rotation matrices. The first is such a matrix $\mathbf{R}$ that

$$\mathbf{U}_A = \mathbf{R}\mathbf{U}_B\mathbf{R}^{\mathrm{T}} \tag{10}$$

The second matrix represents the mutual rotation of variants A and B within the laminate, i.e.,

$$\mathbf{Q} = \mathbf{Q}_A^{\mathrm{T}}\mathbf{Q}_B \tag{11}$$

where the matrices $\mathbf{Q}_A$ and $\mathbf{Q}_B$ are those appearing in (7). The homogenization procedure constructs a set of stress and strain fields homogeneous both in the lamina of variant A and the lamina of variant B. These fields are always chosen such that the compatibility and continuity conditions at the twinning plane are held. For these fields, the procedure evaluates the overall (averaged) elastic strain and the corresponding stored energy of the laminate. In the final step, the elastic coefficients of the laminate are obtained as (numerical) derivatives of the elastic energy function with respect to the averaged strains.

The way in which the twinning influences the symmetry and magnitude of the elastic anisotropy of martensite is shown in Fig. 4, where the Young moduli of austenite, martensite, and twinned martensite (a laminate of type II twins able to form a habit plane with austenite) are compared. The chosen graphical representation is as follows: The 3D surfaces are plots of the Young moduli for uniaxial tensions in directions given by unit vector $\mathbf{n}$, which runs through a unit sphere. The plotted vector quantity is thus $\mathbf{n}E(\mathbf{n})$. The moduli for austenite and a single variant of martensite are shown in the coordinate systems given by principal axes of austenite and martensite, respectively, whereas the moduli of the twinned martensite are plotted in the principal coordinate system of the major variant. Obviously, the difference between Young moduli of the single variant and the twinned martensite is mostly in the symmetry. Similar results can be obtained for shear moduli or for any other representation of the anisotropic elasticity (e.g., surfaces of phase or group velocity of ultrasonic waves, as used in [19]).
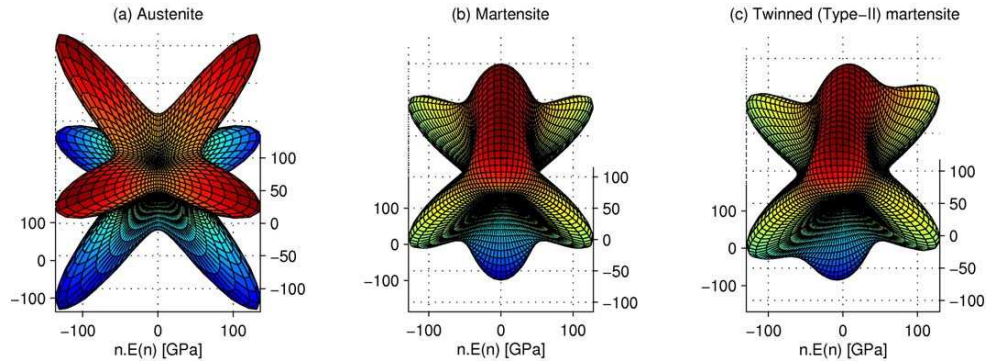
FIGURE 4. Surfaces of Young moduli $\mathbf{n}E(\mathbf{n})$ for all materials involved in the X-interface: **(a)** austenite phase; **(b)** single variant of martensite; **(c)** martensite in the twinned regions

3.3 Results of FEM Modeling

As mentioned in the introduction, to avoid problems with multiscale modeling, the displacement field was decomposed into two parts: transformation and elastic. The nature of the martensitic phase transition enables us to understand these two parts as two independent processes. The first is the deformation according to macroscopic gradients given by the transition, which leads to a discontinuous displacement field over the incompatible interfaces, and the second is the elastic deformation, which ensures the continuity of resulting displacements. Notice that both fields are discontinuous, but their composite is continuous. Whereas the first field is taken directly from the experimental observations, the second one is to be found using FEM.

In the following paragraphs, the whole procedure will be demonstrated for the case of simplified geometry SG 1. Let us denote the macroscopic deformation gradients for austenite, for the A–B laminate, for the A–C laminate, and for the pure variant A by

$$\mathbf{F}_I = \mathbf{I} \tag{12}$$

$$\mathbf{F}_{AB} = \lambda \mathbf{Q}_A \mathbf{U}_A + (1 - \lambda)\mathbf{Q}_B \mathbf{U}_B \tag{13}$$

$$\mathbf{F}_{AC} = \lambda \widehat{\mathbf{Q}}_A \mathbf{U}_A + (1 - \lambda)\mathbf{Q}_B \mathbf{U}_B \tag{14}$$

$$\mathbf{F}_A = \mathbf{Q}_A \mathbf{U}_A \tag{15}$$

Then, four affine transformations can be constructed:

$$\mathbf{y}_I : \mathbf{x} \rightarrow \mathbf{I}\mathbf{x} + \mathbf{b}_I \tag{16}$$

$$\mathbf{y}_{AB} : \mathbf{x} \rightarrow \mathbf{F}_{AB}\mathbf{x} + \mathbf{b}_{AB} \tag{17}$$

$$\mathbf{y}_{AC} : \mathbf{x} \rightarrow \mathbf{F}_{AC}\mathbf{x} + \mathbf{b}_{AC} \tag{18}$$

$$\mathbf{y}_A : \mathbf{x} \rightarrow \mathbf{F}_A\mathbf{x} + \mathbf{b}_A \tag{19}$$

The initial geometry for FEM modeling is obtained by applying these transformations to corresponding domains of the reference configuration. For SG 1, the vectors $\mathbf{b}_I$, $\mathbf{b}_{AB}$, $\mathbf{b}_{AC}$, and $\mathbf{b}_A$ are taken as follows: $\mathbf{b}_I = 0$, $\mathbf{b}_A$ is arbitrary, $\mathbf{b}_{AB}$ and $\mathbf{b}_{AC}$ are chosen so that the entire body remains unbroken over the habit planes (corresponding gradients are compatible, hence such vectors can be found). When the twinned-to-detwinned interfaces are not planes of compatibility, in general, the body splits into two parts. The first one comprises the region of austenite and both twinned regions; the second one contains only the stabilized (detwinned) martensite.

Now, the elasticity problem of putting those parts "back together" must be solved. Elastic moduli are known, so just boundary conditions are to be supplied. These conditions must ensure the uniqueness of the solution and the continuity of the overall displacement field, and thus the integrity of the resulting body. Consider (in the reference configuration) a point $\mathbf{x}_0$ lying in the twinned-to-detwinned interface between the A–B laminate and the pure variant A. In general, points $\mathbf{x}_A = \mathbf{y}_A(\mathbf{x}_0)$ and $\mathbf{x}_{AB} = \mathbf{y}_{AB}(\mathbf{x}_0)$ are different. Therefore the sought elastic displacement field $\mathbf{u}$ must meet the following condition:

$$\mathbf{x}_A + \mathbf{u}(\mathbf{x}_A) = \mathbf{x}_{AB} + \mathbf{u}(\mathbf{x}_{AB}) \tag{20}$$

It can be easily seen that $\mathbf{x}_{AB} = (\mathbf{y}_{AB} \circ \mathbf{y}_A^{-1})(\mathbf{x}_A)$, and the boundary condition in terms of $\mathbf{x}_A$ is

$$\mathbf{u}(\mathbf{x}_A) = (\mathbf{y}_{AB} \circ \mathbf{y}_A^{-1})(\mathbf{x}_A)$$

$$+\mathbf{u}((\mathbf{y}_{AB} \circ \mathbf{y}_A^{-1})(\mathbf{x}_A)) - \mathbf{x}_A \tag{21}$$

This is exactly the boundary condition which was looked for. Similarly, such a condition can be found for the second twinned-to-detwinned interface. To achieve the uniqueness of the solution, the bottom face of the austenite domain was fixed. Hence the multiscale character was fully avoided in the problem formulation, but the non locality of the second term of the right-hand side of (21) is its consequence.

The problem was solved using FEM program COMSOL Multiphysics (formerly Femlab) in connection with the Matlab environment. In Matlab, the geometry was computed as prescribed by the macroscopic morphology. The following FEM computations were done in the COMSOL Structural Mechanics module (Solid, Stress-Strain application mode). For each part of the body in the initial configuration, an independent mesh was needed. To do this, the option *Use Assembly* was enabled. COMSOL was also able to deal with nonlocal couplings through *Extrusion Coupling Variables*. On boundary, where the "gluing" condition was prescribed, the *Boundary Extrusion Coupling Variable* was created according to the known mapping $y_{AB} \circ y_A^{-1}$. For the FEM discretization, the Lagrange cubic finite elements were used. The obtained linear system was solved by the memory-efficient SPOOLES direct solver implemented in COMSOL.

The elastic stress and strain fields were evaluated for all geometries SG 1÷4 and for ratios d_x/L_x running from 0 to 1. An example of the results is shown in Fig. 5. The plotted quantity here is the Von Mises stress (the square root of the second invariant of the stress tensor), evaluated on cuts of the specimen by planes as close as possible to the individ-
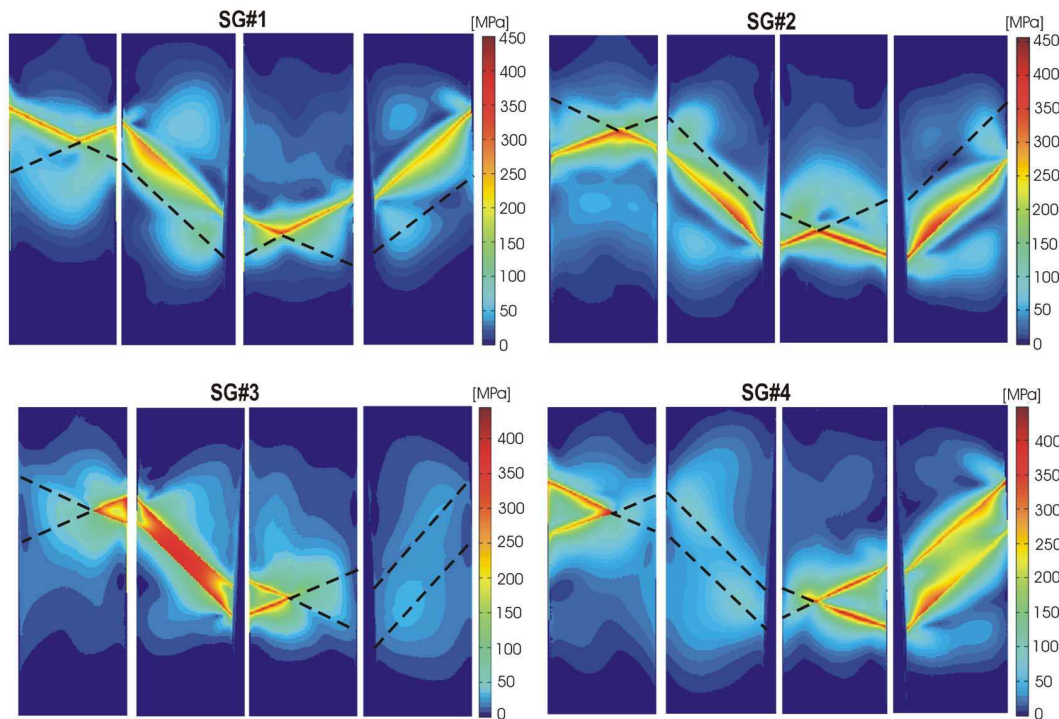

FIGURE 5. Maps of Von Mises stress evaluated on planar cuts closest to the faces of the specimen in simplified geometries SG 1÷4 for $d_x/L_x = 0.65$. The dashed lines denote the intersection of the cutting planes with planes of compatibility (habit planes for SG 1, twinning planes for SG 2, and combinations of habit and twinning planes for SG 3 and SG 4)

ual faces of the specimen.[2] In Fig. 5, the difference between those interfaces (habit planes, twinned-to-detwinned interfaces), which were chosen as planes of compatibility, and those at which the compatibility must be attained by elastic strains is obvious. For SG 1, the elastic strains are concentrated along the twinned-to-detwinned interfaces; for SG 2, a similar concentration is along the austenite-to-martensite interfaces. For SG 3 and SG 4, the maximum stress is localized within the regions surrounded by the interfaces not initially chosen as compatible (this is similiar to [11], where the stress concentration was revealed at the tip of the wedge microstructure). In other words, the obtained elastic fields are strongly influenced by our choice of the simplified geometry (see the last section for a more detailed discussion). In real microstructure (which can be expected to be somewhere between our SGs), both the habit planes and the twinned-to-detwinned interfaces could be elastically strained to achieve full compatibility.

The maximum of the Von Mises stress for all SGs shown in Fig. 5 is nearly the same (approximately 450 MPa). The difference between the geometries can be thus more clearly seen from Fig. 6, where the elastic energy stored in the specimen is plotted as a function of d_x/L_x for all SGs. As expected, the energies of specimens in SG 1 and SG 2 are symmetric about $d_x/L_x = 1/2$. For SG 3 and SG 4, the energy decreases towards the fully compatible configurations. Let us notice here that the crossing lines in the real X-interfaces reported in [8] were located close to the center of the specimen, i.e., close to maximal energies for SG 1 and SG 2.

4. SUMMARY AND DISCUSSION

In this article, a procedure of construction of a mathematical model of an interfacial martensitic microstructure was presented. The examined

---

[2] The initial configuration for which the elasticity problem is solved is given by mapping $\mathbf{y}_{\text{trans}}$, where the faces of the specimen are not planar and the specimen geometry is discontinuous. For this reason, the plotted Von Mises stress was evaluated on cuts of the specimen after the problem solution, i.e., after the "gluing" boundary condition (21) was fulfilled. As the cutting planes, planes as close as possible to the faces of the specimen were chosen. Thus the values of the Von Mises stress in Fig. 5 are very close approximations of the values at the surface
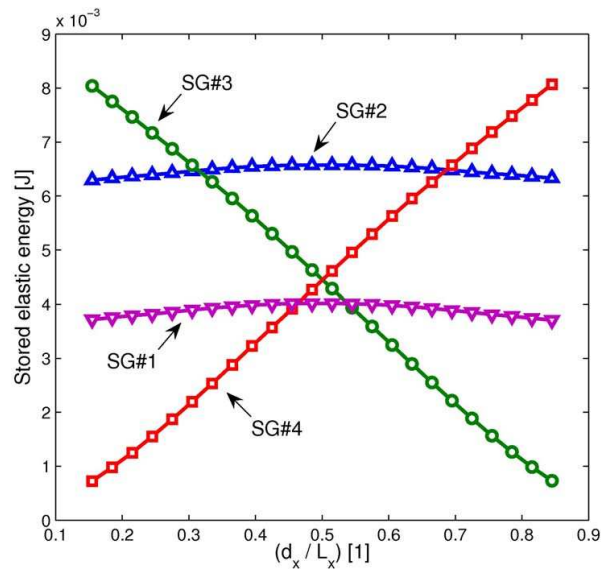

FIGURE 6. Dependence of the elastic energy stored in the specimen on the position of the crossing line for simplified geometries SG 1÷4

material was the Cu-Al-Ni shape memory alloy, and the modeled interfacial microstructure was the X-interface appearing during the shape recovery process in single crystals of this material. From the analysis of the optical micrographs of the real microstructure, the individual twinning systems and variants of martensite forming the microstructure were identified. Based on this identification, the difference of the microstructure from compatibility was analyzed. The elastic strains necessary for the microstructure to achieve compatibility were evaluated by FEM, whereby the elastic coefficients of the twinned regions were evaluated by a homogenization procedure. Four different simplified geometries were used for the calculation. In each of these geometries, the calculation revealed strong concentrations of Von Mises stress along the interfaces not initially chosen as planes of compatibility. Although the simplified geometries are just rough approximations of the real X-interfaces, they enable us to estimate the dependence of the elastic energy stored in the specimen on a chosen geometric parameter (the distance d_x). The presented simulations show that the experimentally observed microstructures are not even local minimizers of the energy (their energy decreases with proper change of parameter

d_x), and thus there must be another explanation for their stability.

On the other hand, the results obtained for SG 1÷4 were strongly influenced by our (artificial) choice of at which planes the compatibility was achieved without elastic strains. Although the differences between the orientation of the habit and twinning planes and those planes that approximate them in our simplified geometries are minimal (less than 2° in the orientation of the normal vectors), the differences in the evaluated elastic fields are tremendous. The internal stress fields in real interfacial microstructures may thus significantly differ from those evaluated for SG 1÷4. However, construction of any more realistic geometry would be extremely complicated, at least for the following three reasons:

1. As the interfacial microstructure grows from the nucleus situated in the corner of the specimen (see [8] for more details), the laminates inside the twinned regions form under (varying) internal stress. For this reason, the laminates cannot be treated as fully homogeneous with the volume fractions given by relations (5) and (6). This may induce additional residual stresses both inside the twinned regions and at the habit plane. However, such variation of λ with the spatial coordinates cannot be evaluated without a complete knowledge of the microstructure's history.

2. As already mentioned, there is no justification for our assumption that the interfaces within the microstructure are exactly planar. Especially close to the crossing line, where all the compatibility conditions (5)–(8) are to be met and where the new martensitic needles nucleate (again, see [8] for more details), the shapes can be completely general. However, the real shapes of the interfaces can be determined neither experimentally (from optical micrographs, only the intersections of the interfaces with the surfaces of the specimen can be obtained; ultrasonic methods do not have sufficient resolution) nor theoretically (as the optimality criterion for the X-interfaces, which are *a priori* not minimizers of energy, is unknown).

3. The multiscale character cannot be fully avoided. Along the twinned-to-detwinned

interfaces, the stress fields are not homogeneously distributed, but concentrated around the tips of individual martensitic needles nucleating at the crossing line and growing toward the lateral faces of the specimen. Moreover, the exact shapes of the needles are not known, and their determination is complicated for the same reasons as discussed in point 2.

Solution of the problems resulting from the preceding three points will be the subject of the authors' future work.

ACKNOWLEDGMENT

REFERENCES

1. Otsuka, K., and Wayman, C., Eds., *Shape Memory Materials*. Cambridge University Press, Cambridge, 1998.

2. Bhattacharya, K., *Microstructure of Martensite.* Oxford University Press, New York, 2003.

3. Ball, J. M., and James, R. D., Fine phase mixtures as minimizers of energy. *Arch. Rat. Mech. Anal.* **100**:13–52, 1987.

4. Ball, J. M., and James, R. D., Proposed experimental tests of theory of fine microstructure and the two-well problem. *Philos. Trans.* **338**:389–450, 1992.

5. Dolzmann, G., *Variational Methods for Crystalline Microstructure – Analysis and Computation.* Springer, Berlin, 2003.

6. Bhattacharya, K., Li, B., and Luskin, M., The simply laminated microstructure in martensitic crystals that undergo a cubic to orthorhombic phase trans formation. *Arch. Rat. Mech. Anal.* **149**:123–154, 1999.

7. Novák, V., Šittner, P., Ignacová, S., and Černoch, T., Transformation behavior of prism shaped shape memory alloy single crystals. *Mater. Sci. Eng. A.* **A438-440**:755–762, 2006.

8. Seiner, H., Sedlák, P., and Landa, M., Shape recovery mechanism observed in single crystals of Cu-Al-Ni shape memory alloy. *Phase Trans.* **81**:537–551, 2008.

9. Basinski, Z. S., and Christian, J. W., Experiments on the martensitic trasformation in single crystals of indium-thallium alloys. *Acta Metall.* **2**:148–166, 1954.

10. Ruddock, G., A Microstructure of martensite which is not a minimiser of energy: The X-interface, *Arch. Rat. Mech. Anal.* **127**:1–39, 1994.

11. Balandraud, X., and Zanzotto, G., Stressed microstructures in thermally induced M9R-M18R martensites. *J. Mech. Phys. Solids.* **55**:194–224, 2007.

12. Turteltaub, S., and Suiker, A. S. J., A multiscale thermomechanical model for cubic to tetragonal martensitic phase transformations. *Int. J. Solids Struct.* **43**:4509–4545, 2006.

13. Gao, X., Huang, H., and Brinson, L. C., A multivariant micromechanical model for SMAs, part 1. Crystallographic issues for single crystal model. *Int. J. Plasticity.* **16**:1345–1369, 2000.

14. Patoor, E., Lagoudas, D. C., Entchev, P. B., Brinson, L. C., and Gao, X., Shape memory alloys, part I: General properties and modeling of single crystals. *Mech. Mater.* **38**:391–429, 2006.

15. Lagoudas, D. C., Entchev, P. B., Popov, P., Patoor, E., Brinson, L. C., and Gao, X., Shape memory alloys, part II: Modeling of polycrystals. *Mech. Mater.* **38**:430–462, 2006.

16. Popov, P., and Lagoudas, D. C., A 3-D constitutive model for shape memory alloys incorporating pseudoelasticity and detwinning of self-accommodated martensite.*Int. J. Plasticity.*

23:1679–1720, 2007.

17. Hane, K. F., Microstructures in Thermoelastic Martensites. Ph.D. Thesis, University of Minnesota, 1998.

18. Chu, C-H., and James, R. D., Analysis of microstructures in Cu-14.0%Al-3.9%Ni by energy minimization. *J De Phys. IV*. **JP5**:143–149, 1995.

19. Sedlák, P., Seiner, H., Landa, M., Novák, V., Šittner, P., and Manosa, L., Elastic constants of BCC austenite and 2H orthorombic martensite in CuAlNi shape memory alloy. *Acta Mater.* **53**:3643–3661, 2005.

20. Brinson, L. C., and Lammering, R., Finite element analysis of the behavior of shape memory alloys and their applications. *Int. J. Solids Struct.* **30**:3261–3280, 1993.

21. Auricchio, F., and Petrini, L., A three-dimensional model describing stress-temperature induced solid phase transformations: Solution algorithm and boundary value problem. *Int. J. Numer. Meth. Eng.* **61**:807–836, 2004.

22. Stupkiewicz, S., Maciewski, G., and Petryk, H., Low-energy morphology of the interface layer between austenite and twinned martensite. *Acta Mater.* **55**:6292–6306, 2007.

23. Musgrave, M. J. P., *Crystal Acoustics*. Holden-Day, San Francisco, 1970.

24. Nayfeh, A. H., *Wave Propagation in Layered Anisotropic Media.* North-Holland, Amsterdam, 1995.

25. Seiner, H., Dynamic and transient phenomena in single crystals of shape memory alloys, Ph.D. thesis, Czech Technical University in Prague, 2008.

26. Landa, M., Sedlák, P., Seiner, H., Heller, L., Bicanová, L., Šittner, P., and Novák, V., Modal resonant ultrasound spectroscopy for ferroelastics. *Appl. Phys. A*. **93**:557–567, 2009.